

An analytical model for the pull-out of rigid anchors

R. BALLARINI,¹ L.M. KEER² and S.P. SHAH²

¹ *Department of Civil Engineering, Case Western Reserve University, Cleveland, OH 44106, USA;*

² *Department of Civil Engineering, Northwestern University, Evanston, IL 66201, USA*

Received 30 September 1986; accepted 11 December 1986

Abstract

A linear elastic fracture mechanics model is presented for the pull-out failure caused by a rigid anchor embedded in a brittle material. The anchor is modeled as a vertically loaded, partly bonded rigid plate in an elastic half-space, and failure is assumed to arise from cracking which emanates from the edges of the plate. The two-dimensional elasticity problem is reduced to solving numerically a system of coupled singular integral equations. Stress intensity factors are presented for several combinations of load geometry, crack length, crack extension angle, and embedment depth. The stress intensity factors are used to construct crack paths and to determine the stability of crack propagation.

1. Introduction

The pull-out failure of embedded anchors is an important consideration for many critical design situations. Anchor bolts are often used as connections in concrete structures, roof bolts in rock tunnels, and tie backs in rocks. The problem to be studied in this paper is the pull-out of a two-dimensional anchor. A first attempt at solution to such a problem was made by Miller and Keer [1], who used a complex variables approach to quantify the cracking that might develop at the tip of an anchor being pulled vertically in an infinite elastic medium. This solution did not model the exact conditions for two reasons:

1. The loaded surface of the half-space was approximated by concentrated loads in an infinite space.
2. The cracks that branched from the anchor were assumed to be straight.

Within this context the Miller-Keer solution was an improvement on earlier analytical studies that focused primarily on stress distributions and load deflection behavior [2,3,4,5]. A later paper by Ballarini et al. [6] presented the physical results to the problem to be discussed herein. Since for brevity the detailed analysis was suppressed there, it is appropriate and useful to describe the mathematical details so that researchers could use the techniques to solve related useful problems. In this paper the free surface effect is incorporated and crack paths are predicted so that crack growth near the surface loads can be correctly described.

2. Formulation

The problem (see Fig. 1) is formulated in terms of the complex potentials of Muskhelishvili [7]. The stresses and displacements can be expressed in terms of the analytic functions Φ and Ψ as

$$\sigma_{xx} + \sigma_{yy} = 4 \operatorname{Real}[\Phi(z)] \quad (1)$$

$$\sigma_{yy} - i\sigma_{xy} = \Phi(z) + \overline{\Phi(z)} + z\overline{\Phi'(z)} + \overline{\Psi(z)} \quad (2)$$

$$2\mu \left(\frac{\partial u}{\partial x} + i \frac{\partial v}{\partial x} \right) = \kappa\Phi(z) - \overline{\Phi(z)} - z\overline{\Phi'(z)} - \overline{\Psi(z)} \quad (3)$$

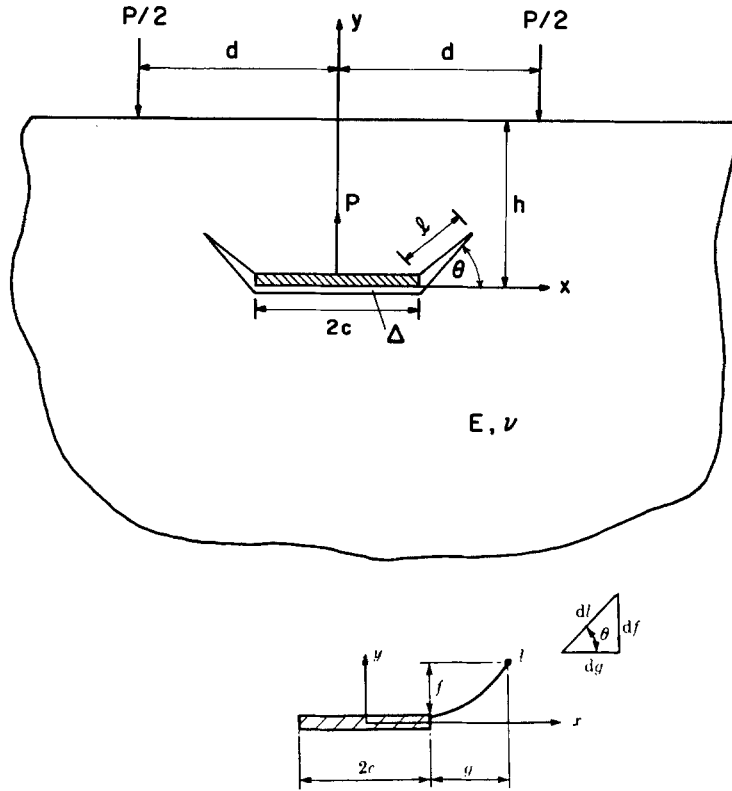


Fig. 1. Mathematical model of embedded anchor (for pre-cracking solution $l = 0$).

where $i = \sqrt{-1}$, $z = x + iy$, μ is the shear modulus, $\kappa = 3 - 4\nu$ for plane strain and $\kappa = (3 - \nu/1 + \nu)$ for plane stress, ν being Poisson's ratio. Primes denote differentiation with respect to z , and bars imply complex conjugation. The anchor is modeled as a vertically loaded, partly bonded rigid plate in an elastic half-space. Failure is assumed to arise from cracking which emanates from the corners of the plate. The boundary conditions along the plate corresponding to this problem are

$$2\mu \left(\frac{\partial u}{\partial x} + i \frac{\partial v}{\partial x} \right)^+ = 0 \quad (\text{bonded upper portion}) \tag{4}$$

and

$$(\sigma_{yy} - i\sigma_{xy})^- = 0 \quad (\text{unbonded lower portion}) \tag{5}$$

where the superscripts + and - refer to the upper and lower surfaces of the plate, respectively. Along the growing cracks,

$$\sigma_{\phi\phi} - i\sigma_{\rho\phi} = 0 \quad (\text{stress-free crack surface}), \tag{6}$$

where $\sigma_{\phi\phi}$ and $\sigma_{\rho\phi}$ represent the normal and shear stresses along the crack surfaces.

3. Pre-cracking solution

In this section a solution is developed for the case where the cracks are not present ((6) is not enforced). The method of solution relies on the Green's functions for a dislocation in a

half-space and for a point force in a half-space. The solution to the problem of a discrete dislocation in a half-space is well known [8], and may be written in terms of three potentials. The two potentials Φ_{DW} and Ψ_{DW} which are given by

$$\Phi_{DW}(z) = \frac{\beta}{z - z_1} \quad (7)$$

$$\Phi_{DW}(z) = \frac{\bar{\beta}}{z - z_1} + \frac{\beta \bar{z}_1}{(z - z_1)^2} \quad (8)$$

provide the necessary displacement jumps corresponding to a dislocation at the point z_1 . The constant β is defined as

$$\beta = \frac{\mu e^{i\theta}}{\pi i(\kappa + 1)} \{ [u_r] + i[v_\theta] \} \quad (9)$$

where $[u_r]$ and $[v_\theta]$ represent the magnitudes of the displacement jumps. An additional potential, which is required to clear the surface tractions, is most conveniently written in terms of Φ_{DW} and ψ_{DW} (see e.g. [9]) as

$$\Phi_{DC}(z) = \begin{cases} -\overline{\Phi_{DW}(\bar{z})} - z\overline{\Phi'_{DW}(\bar{z})} - \overline{\Psi_{DW}(\bar{z})} & \text{Im}(z) < 0 \\ \Phi_{DW}(z) & \text{Im}(z) > 0 \end{cases} \quad (10)$$

Here, a half-plane continuation has been used, and thus the stresses and displacements due to Φ_{DC} are given as [7]

$$\sigma_{xx} + \sigma_{yy} = 4 \text{Real}[\Phi_{DC}(z)] \quad (11)$$

$$\sigma_{yy} - i\sigma_{xy} = \Phi_{DC}(z) - \overline{\Phi_{DC}(\bar{z})} + (z - \bar{z})\overline{\Phi'_{DC}(\bar{z})} \quad (12)$$

$$2\mu \left(\frac{\partial u}{\partial x} + i \frac{\partial v}{\partial x} \right) = \kappa \Phi_{DC}(z) + \overline{\Phi_{DC}(\bar{z})} - (z - \bar{z})\overline{\Phi'_{DC}(\bar{z})}. \quad (13)$$

The same procedure is also performed for the concentrated forces. For this case the potentials

$$\Phi_{CW} = \frac{\alpha}{z - z_0} \quad (14)$$

$$\Psi_{CW} = \frac{-\kappa \bar{\alpha}}{z - z_0} + \frac{\alpha \bar{z}_0}{(z - z_0)^2} \quad (15)$$

provide the necessary stress jump condition corresponding to a concentrated force at the point z_0 . The constant α is defined as

$$\alpha = \frac{-(F_x + iF_y)}{2\pi(\kappa + 1)} \quad (16)$$

where F_x and F_y represent the x and y components of the force, respectively. The additional potential which is required to clear the surface tractions is written as

$$\Phi_{CC}(z) = \begin{cases} -\overline{\Phi_{CW}(\bar{z})} - z\overline{\Phi'_{CW}(\bar{z})} - \overline{\Psi_{CW}(\bar{z})} & \text{Im}(z) < 0 \\ \Phi_{CW}(z) & \text{Im}(z) > 0 \end{cases} \quad (17)$$

and the displacements and stresses due to Φ_{CC} are given by (11)–(13) where Φ_{CC} replaces Φ_{DC} . The relevant stresses and displacements that arise from the concentrated forces on the

surface, a dislocation at the point z_1 and a concentrated force at the point z_0 become

$$\begin{aligned} \sigma_{yy} - i\sigma_{xy} = & \frac{iP}{4\pi} \left\{ \frac{1}{z-d} + \frac{1}{z+d} - \frac{1}{\bar{z}-d} - \frac{1}{\bar{z}+d} + (z-\bar{z}) \left[\frac{1}{(\bar{z}-d)^2} + \frac{1}{(\bar{z}+d)^2} \right] \right\} \\ & + \beta \left\{ \frac{1}{z-z_1} - \frac{1}{z-\bar{z}_1} + \frac{1}{\bar{z}-\bar{z}_1} - \frac{1}{\bar{z}-z_1} + \frac{2(\bar{z}_1-z_1)(z-\bar{z})}{(\bar{z}-z_1)^3} \right\} \\ & + \bar{\beta} \left\{ \frac{(\bar{z}_1-z_1)}{(z-\bar{z}_1)^2} - \frac{(\bar{z}_1-z_1)}{(\bar{z}-\bar{z}_1)^2} - \frac{(z-\bar{z})}{(\bar{z}-\bar{z}_1)^2} + \frac{(z-\bar{z})}{(\bar{z}-z_1)^2} \right\} \\ & + \alpha \left\{ \frac{1}{z-z_0} + \frac{\kappa}{z-\bar{z}_0} - \frac{\kappa}{\bar{z}-\bar{z}_0} - \frac{1}{\bar{z}-z_0} + \frac{2(\bar{z}_0-z_0)(z-\bar{z})}{(\bar{z}-z_0)^3} \right\} \\ & + \bar{\alpha} \left\{ \frac{(\bar{z}_0-z_0)}{(z-\bar{z}_0)^2} - \frac{(\bar{z}_0-z_0)}{(\bar{z}-\bar{z}_0)^2} - \frac{(z-\bar{z})}{(\bar{z}-\bar{z}_0)^2} - \frac{\kappa(z-\bar{z})}{(\bar{z}-z_0)^2} \right\} \end{aligned} \quad (18)$$

$$\begin{aligned} 2\mu \left(\frac{\partial u}{\partial x} + i \frac{\partial v}{\partial x} \right) = & \frac{iP}{4\pi} \left\{ \frac{\kappa}{z-d} + \frac{\kappa}{z+d} + \frac{1}{\bar{z}-d} + \frac{1}{\bar{z}+d} - (z-\bar{z}) \left[\frac{1}{(\bar{z}-d)^2} + \frac{1}{(\bar{z}+d)^2} \right] \right\} \\ & + \beta \left\{ \frac{\kappa}{z-z_1} - \frac{\kappa}{z-\bar{z}_1} - \frac{1}{\bar{z}-\bar{z}_1} + \frac{1}{\bar{z}-z_1} - \frac{2(\bar{z}_1-z_1)(z-\bar{z})}{(\bar{z}-z_1)^3} \right\} \\ & + \bar{\beta} \left\{ \frac{\kappa(\bar{z}_1-z_1)}{(z-\bar{z}_1)^2} + \frac{(\bar{z}_1-z_1)}{(\bar{z}-\bar{z}_1)^2} + \frac{(z-\bar{z})}{(\bar{z}-\bar{z}_1)^2} - \frac{(z-\bar{z})}{(\bar{z}-z_1)^2} \right\} \\ & + \alpha \left\{ \frac{\kappa}{z-z_0} + \frac{\kappa^2}{z-\bar{z}_0} + \frac{\kappa}{\bar{z}-\bar{z}_0} + \frac{1}{\bar{z}-z_0} - \frac{2(\bar{z}_0-z_0)(z-\bar{z})}{(\bar{z}-z_0)^3} \right\} \\ & + \bar{\alpha} \left\{ \frac{\kappa(\bar{z}_0-z_0)}{(z-\bar{z}_0)^2} + \frac{(\bar{z}_0-z_0)}{(\bar{z}-\bar{z}_0)^2} + \frac{(z-\bar{z})}{(\bar{z}-\bar{z}_0)^2} + \frac{\kappa(z-\bar{z})}{(\bar{z}-z_0)^2} \right\}. \end{aligned} \quad (19)$$

The discrete dislocation at z_1 and the concentrated force at z_0 are replaced with a distribution of dislocations, $\beta(\rho) d\rho$, and body forces, $\alpha(\xi) d\xi$, defined as

$$\beta(\rho) = \frac{\mu e^{i\theta}}{\pi i(\kappa+1)} \frac{\partial}{\partial \rho} \{ [u_r] + i[v_\theta] \} \quad (20)$$

$$\alpha(\xi) = \frac{-1}{2\pi(\kappa+1)} \frac{\partial}{\partial \xi} (F_x + iF_y) \quad (21)$$

along the lines $z_1 = \rho - ih$ and $z_0 = \xi - ih$, ($-c \leq \rho, \xi \leq c$). This representation enables one to write equations for boundary conditions (4) and (5). In particular, the potentials become integral expressions and the relevant stresses and displacements become

$$\begin{aligned} \sigma_{yy} - i\sigma_{xy} = & \frac{iP}{4\pi} \left\{ \frac{1}{z-d} + \frac{1}{z+d} - \frac{1}{\bar{z}-d} - \frac{1}{\bar{z}+d} + (z-\bar{z}) \left[\frac{1}{(\bar{z}-d)^2} + \frac{1}{(\bar{z}+d)^2} \right] \right\} \\ & + \int_{-c}^c \alpha(\xi) \left[\frac{1}{z-\xi+ih} + \frac{\kappa}{z-\xi-ih} - \frac{\kappa}{\bar{z}-\xi-ih} - \frac{1}{\bar{z}-\xi+ih} \right] \end{aligned}$$

$$\begin{aligned}
 & + \frac{4ih(z-\bar{z})}{(\bar{z}-\xi+ih)^3} \Big] d\xi \\
 & + \int_{-c}^c \overline{\alpha(\xi)} \left[\frac{2ih}{(z-\xi-ih)^2} - \frac{2ih}{(\bar{z}-\xi-ih)^2} - \frac{(z-\bar{z})}{(\bar{z}-\xi-ih)^2} - \frac{\kappa(z-\bar{z})}{(\bar{z}-\xi+ih)^2} \right] d\xi \\
 & + \int_{-c}^c \beta(\rho) \left[\frac{1}{z-\rho+ih} - \frac{1}{z-\rho-ih} + \frac{1}{\bar{z}-\rho-ih} - \frac{1}{\bar{z}-\rho+ih} \right. \\
 & \left. + \frac{4ih(z-\bar{z})}{(\bar{z}-\rho+ih)^3} \right] d\rho + \int_{-c}^c \overline{\beta(\rho)} \left[\frac{2ih}{(z-\rho-ih)^2} - \frac{2ih}{(\bar{z}-\rho-ih)^2} \right. \\
 & \left. - \frac{(z-\bar{z})}{(\bar{z}-\rho-ih)^2} + \frac{(z-\bar{z})}{(\bar{z}-\rho+ih)^2} \right] d\rho \tag{22}
 \end{aligned}$$

$$\begin{aligned}
 2\mu \left(\frac{\partial u}{\partial x} + i \frac{\partial v}{\partial x} \right) &= \frac{iP}{4\pi} \left\{ \frac{\kappa}{z-d} + \frac{\kappa}{z+d} + \frac{1}{\bar{z}-d} + \frac{1}{\bar{z}+d} - (z-\bar{z}) \left[\frac{1}{(\bar{z}-d)^2} + \frac{1}{(\bar{z}+d)^2} \right] \right\} \\
 & + \int_{-c}^c \alpha(\xi) \left[\frac{\kappa}{z-\xi+ih} + \frac{\kappa^2}{z-\xi-ih} + \frac{\kappa}{\bar{z}-\xi-ih} + \frac{1}{\bar{z}-\xi+ih} - \frac{4ih(z-\bar{z})}{(\bar{z}-\xi+ih)^2} \right] d\xi \\
 & + \int_{-c}^c \overline{\alpha(\xi)} \left[\frac{2ih\kappa}{(z-\xi-ih)^2} + \frac{2ih}{(\bar{z}-\xi-ih)^2} + \frac{(z-\bar{z})}{(\bar{z}-\xi-ih)^2} + \frac{\kappa(z-\bar{z})}{(\bar{z}-\xi+ih)^2} \right] d\xi \\
 & + \int_{-c}^c \beta(\rho) \left[\frac{\kappa}{z-\rho+ih} - \frac{\kappa}{z-\rho-ih} - \frac{1}{\bar{z}-\rho-ih} + \frac{1}{\bar{z}-\rho+ih} - \frac{4ih(z-\bar{z})}{(\bar{z}-\rho+ih)^3} \right] d\rho \\
 & + \int_{-c}^c \overline{\beta(\rho)} \left[\frac{2ih\kappa}{(z-\rho-ih)^2} + \frac{2ih}{(\bar{z}-\rho-ih)^2} + \frac{(z-\bar{z})}{(\bar{z}-\rho-ih)^2} - \frac{(z-\bar{z})}{(\bar{z}-\rho+ih)^2} \right] d\rho. \tag{23}
 \end{aligned}$$

The expressions in (4) and (5) must be evaluated as the boundary values of (22) and (23) as z approaches the anchor from the top or from the bottom. The Plemelj formulae [7] are employed to obtain the boundary values and from boundary conditions (4) and (5) the following system of coupled singular integral equations are obtained

$$\begin{aligned}
 & \int_{-c}^c \alpha(\xi) \left\{ \frac{\kappa-1}{\xi-x} + K_1(x, \xi) \right\} d\xi + \int_{-c}^c \overline{\alpha(\xi)} K_2(x, \xi) d\xi \\
 & + \pi i(\kappa+1)\alpha(x) + \int_{-c}^c \beta(\rho) \left\{ \frac{-2}{\rho-x} + K_3(x, \rho) \right\} d\rho \\
 & + \int_{-c}^c \overline{\beta(\rho)} K_4(x, \rho) d\rho + f_1(x) = 0 \quad -c \leq x \leq c \tag{24}
 \end{aligned}$$

$$\begin{aligned}
 & \int_{-c}^c \alpha(\xi) \left\{ \frac{-2\kappa}{\xi-x} + K_5(x, \xi) \right\} d\xi + \int_{-c}^c \overline{\alpha(\xi)} K_6(x, \xi) d\xi \\
 & + \int_{-c}^c \beta(\rho) \left\{ \frac{1-\kappa}{\rho-x} + K_7(x, \rho) \right\} d\rho + \int_{-c}^c \overline{\beta(\rho)} K_8(x, \rho) d\rho \\
 & - \pi i(\kappa+1)\beta(x) + f_2(x) = 0 \quad -c \leq x \leq c \tag{25}
 \end{aligned}$$

where $K_1 \dots K_8$, f_1 and f_2 are given in Appendix A. To ensure uniqueness the following

subsidiary conditions must be enforced

$$\int_{-c}^c \alpha(\xi) d\xi = \frac{P}{2\pi i(\kappa + 1)} \quad (\text{equilibrium of plate}) \quad (26)$$

$$\int_{-c}^c \beta(\rho) d\rho = 0 \quad (\text{crack closure}). \quad (27)$$

4. Physical quantities

All important physical quantities can be evaluated after (24)–(27) have been solved for the unknowns $\alpha(\xi)$ and $\beta(\rho)$. In particular, the stresses are given by (22) and the relative displacements representing the gap between the anchor and the elastic medium are given by

$$[u_x] + i[u_y] = \frac{\pi i(\kappa + 1)}{\mu} \int_x^c \beta(\rho) d\rho \quad (28)$$

5. Whole space solution

To perform the numerical integration involved in (24)–(27), the behavior of the functions α and β must be determined. Their behavior is obtained by letting depth of the anchor approach infinity and extracting the whole space solution. This procedure leads to a Hilbert problem whose solution is

$$\alpha(x) = \frac{P}{8\pi^2(\kappa + 1)} \left\{ (1 + i\sqrt{\kappa})(c+x)^{-\gamma_1}(c-x)^{\gamma_1-1} e^{i\pi(\gamma_1-1)} \right. \\ \left. + (1 - i\sqrt{\kappa})(c+x)^{-\gamma_2}(c-x)^{\gamma_2-1} e^{i\pi(\gamma_2-1)} \right\} \quad (29)$$

$$\beta(x) = \frac{P}{8\pi^2(\kappa + 1)} \left\{ (-\kappa + i\sqrt{\kappa})(c+x)^{-\gamma_1}(c-x)^{\gamma_1-1} e^{i\pi(\gamma_1-1)} \right. \\ \left. + (-\kappa - i\sqrt{\kappa})(c+x)^{-\gamma_2}(c-x)^{\gamma_2-1} e^{i\pi(\gamma_2-1)} \right\} \quad (30)$$

where

$$\gamma_1 = \frac{1}{4} + \frac{\log \kappa}{4\pi i} \quad (31)$$

$$\gamma_2 = \frac{3}{4} + \frac{\log \kappa}{4\pi i}. \quad (32)$$

This solution agrees with the result obtained by D.I. Sherman [10].

6. Numerical results

Equations (24)–(27) were solved numerically using the method proposed by Miller and Keer [11]. All results presented in the mathematical analysis are for plane strain with $\nu = 0.2$.

Figures 2–5 are contour plots of maximum and minimum principal stresses. The results presented are all for the case $h = 2c$. It can be seen from these figures that the location of the support reactions significantly influences the stress fields. In all cases very high stresses are observed near the tips of the anchor. As a result of the high compressive stresses produced by the concentrated forces, the maximum principal stresses decay faster when the support

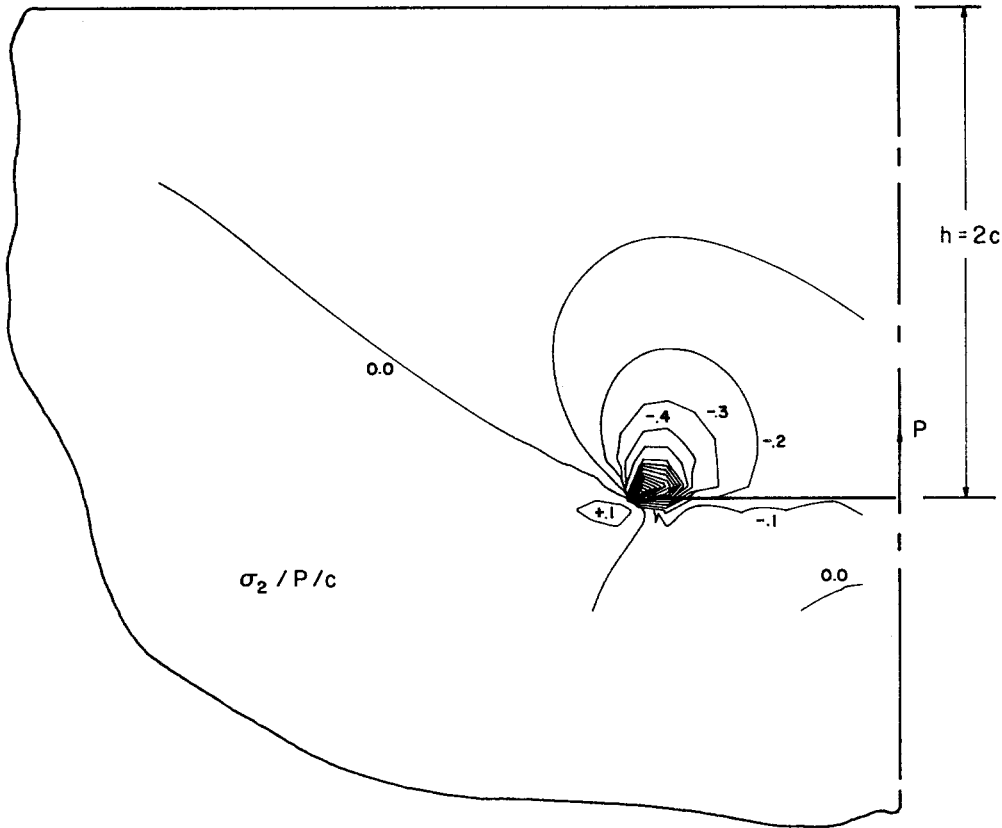


Fig. 2. Contours of minimum principal stresses ($h = 2c$) - (from [6]).

reactions are present than when they are absent. The minimum principal stresses are also strongly influenced by the support reactions. For the case when the support reactions are absent, large compressive stresses, which decay rapidly away from the edges of the anchor are observed. On the other hand, when the support reactions are present, very high compressive stresses exist in a region extending from the tips of the anchor to the supports.

Table 1 illustrates changes in the compliance as the embedment and support distances change. The compliance increases in magnitude as (1) the depth of the embedment decreases and (2) as the support distance increases. Thus, changes in the experiment geometry may strongly influence the failure mechanisms.

Table 1. Compliance as function of geometry.

$\frac{h}{2c}$	$\frac{d}{2c}$	$\frac{\mu\Delta}{p}$
0.75	Concentrated forces not present	0.368
1.00	Concentrated forces not present	0.332
1.25	Concentrated forces not present	0.309
∞	Concentrated forces not present	0.210
0.75	0.75	0.186
0.75	1.50	0.320
1.00	1.00	0.208
1.00	1.50	0.272
1.25	1.25	0.215

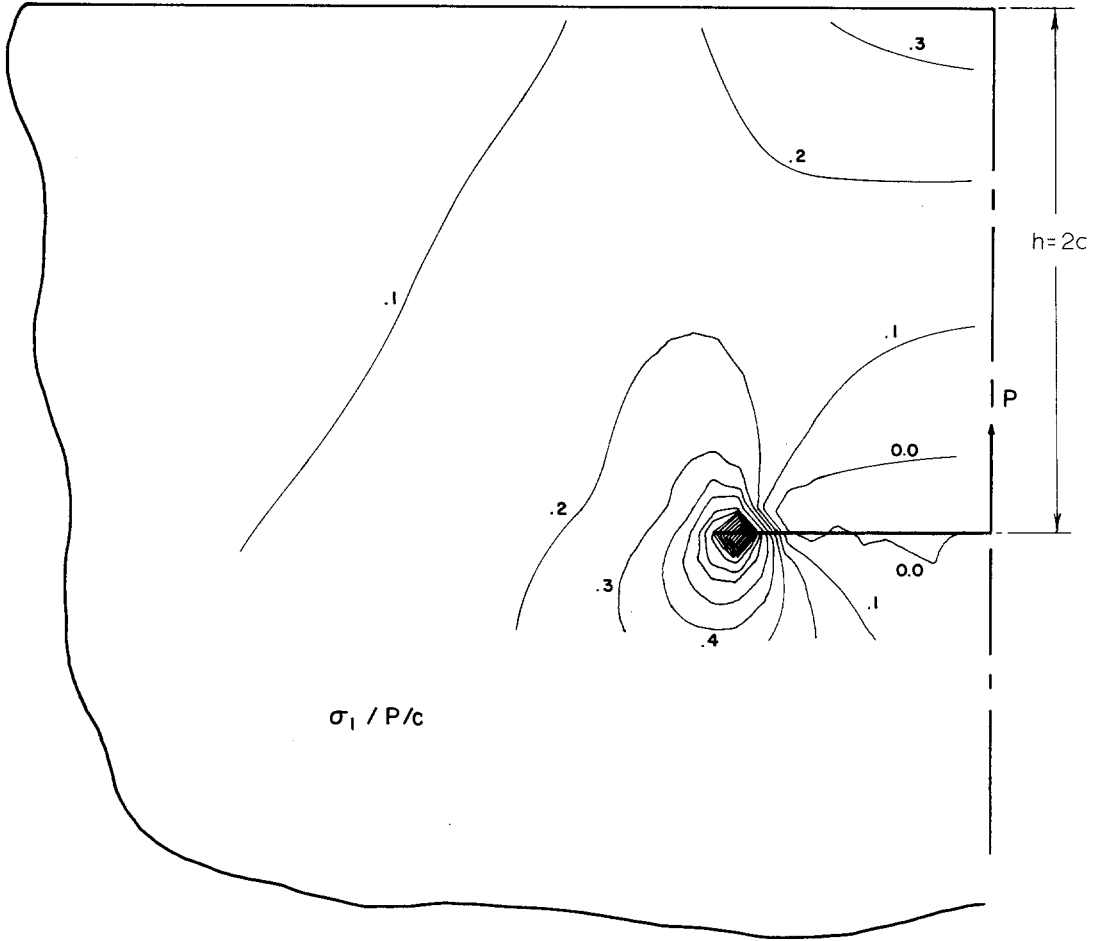


Fig. 3. Contours of maximum principal stresses ($h = 2c$).

7. Post cracking solution

A method of solution similar to the pre-cracking case is given next for the case where the cracks are present. This problem requires additionally that (6) be satisfied along the extending cracks.

Using a half-plane continuation, the following expression for the extended crack stresses can be determined

$$\sigma_{\phi\phi} - i\sigma_{\rho\phi} = \Phi(z) + (1 - e^{-2i\theta})\overline{\Phi(z)} - e^{-2i\theta}\Phi(\bar{z}) + e^{-2i\theta}(z - \bar{z})\overline{\Phi'(z)}. \tag{33}$$

Due to the symmetry of the problem the constants α and β appearing in the preceding solution are replaced by α at $z_0 = \xi - ih$, $-\bar{\alpha}$ at $-\bar{z}_0 = -\xi - ih$ ($0 \leq \xi \leq c$), β at $z_1 = \rho - ih$, $-\bar{\beta}$ at $-\bar{z}_1 = -\rho - ih$ ($0 \leq \rho \leq c$). To satisfy (6) the cracks are modeled as distributions of symmetric dislocations as follows: ψ at $z_2 = c - ih + \tau e^{i\theta}$ and $-\bar{\psi}$ at $-\bar{z}_2 = -c - ih - \tau e^{-i\theta}$, where

$$\psi(\tau) = \frac{\mu e^{i\theta}}{\pi i(\kappa + 1)} \frac{\partial}{\partial \tau} \{ [u_r] + i[v_\theta] \}. \tag{34}$$

Following the same procedure as for the pre-cracking solution and enforcing (6) the

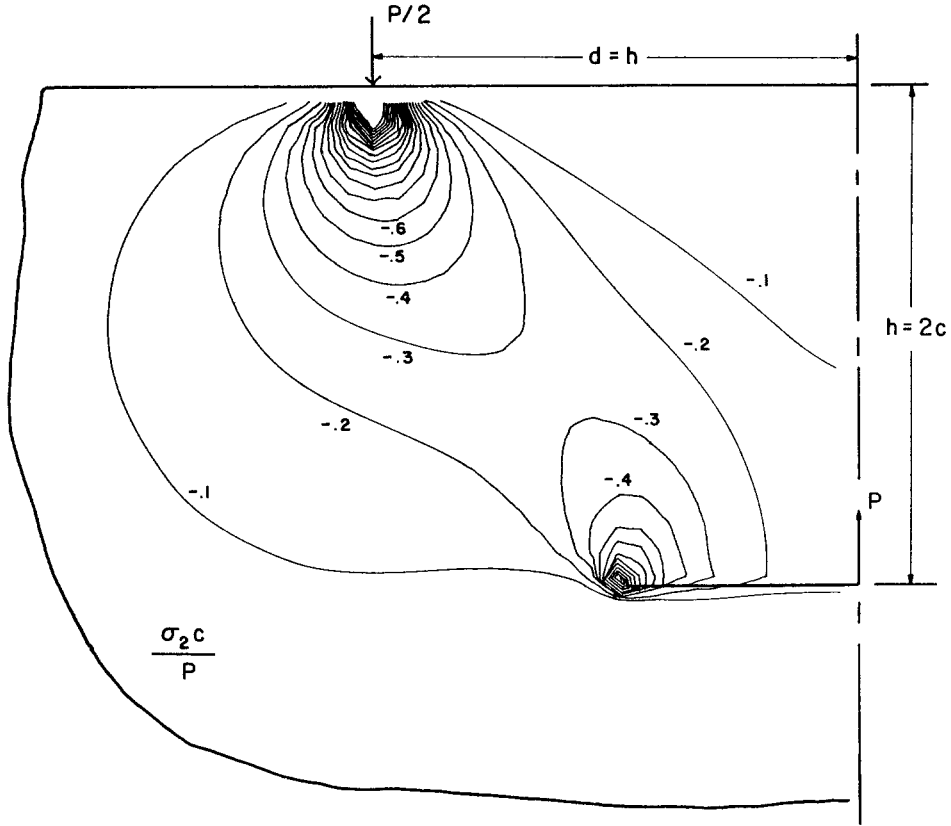


Fig. 4. Contours of minimum principal stresses ($h = d = 2c$) (from [6]).

following system of integral equations is obtained

$$\begin{aligned}
 & \int_0^c \alpha(\xi) \left\{ \frac{\kappa-1}{\xi-x} + K_1(x, \xi) - K_2(x, -\xi) \right\} d\xi + \int_0^c \overline{\alpha(\xi)} \{ K_2(x, \xi) - K_1(x, -\xi) \} d\xi \\
 & + \pi i(\kappa+1)\alpha(x) + \int_0^c \beta(\rho) \left\{ \frac{-2}{\rho-x} + K_3(x, \rho) - K_4(x, -\rho) \right\} d\rho \\
 & + \int_0^c \beta(\rho) \{ K_4(x, \rho) - K_3(x, -\rho) \} d\rho \\
 & + \int_0^l \psi(\tau) K_9(x, \tau) d\tau + \int_0^l \overline{\psi(\tau)} K_{10}(x, \tau) d\tau + f_1(x) = 0 \quad -c \leq x \leq c \quad (35)
 \end{aligned}$$

$$\begin{aligned}
 & \int_0^c \alpha(\xi) \left\{ \frac{-2\kappa}{\xi-x} + K_5(x, \xi) - K_6(x, -\xi) \right\} d\xi + \int_0^c \overline{\alpha(\xi)} \{ K_6(x, \xi) - K_5(x, -\xi) \} d\xi \\
 & + \int_0^c \beta(\rho) \left\{ \frac{1-\kappa}{\rho-x} + K_7(x, \rho) - K_8(x, -\rho) \right\} d\rho + \int_0^c \overline{\beta(\rho)} \{ K_8(x, \rho) - K_7(x, -\rho) \} d\rho \\
 & - \pi i(\kappa+1)\beta(x) + \int_0^l \psi(\tau) K_{11}(x, \tau) d\tau + \int_0^l \overline{\psi(\tau)} K_{12}(x, \tau) d\tau + f_2(x) = 0 \\
 & -c \leq x \leq c \quad (36)
 \end{aligned}$$

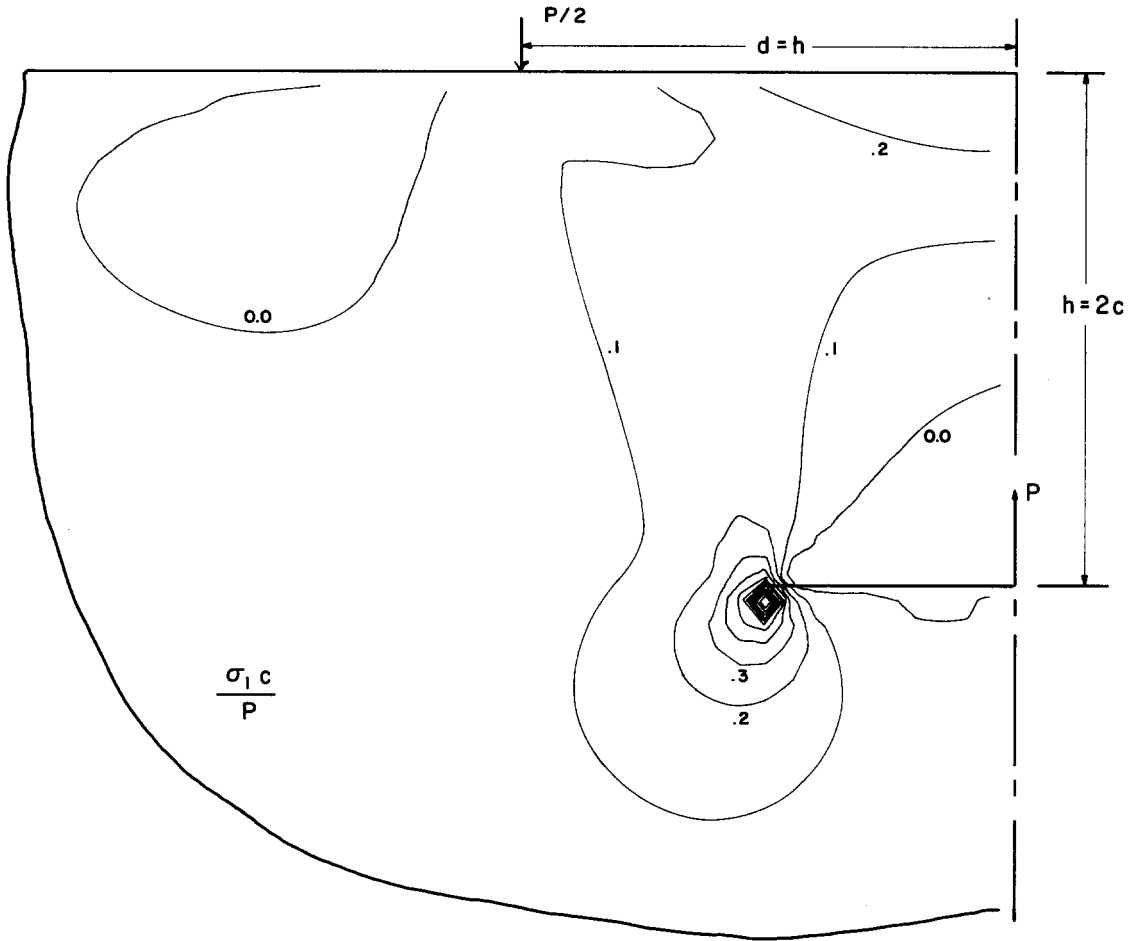


Fig. 5. Contours of maximum principal stresses ($h = d = 2c$).

$$\begin{aligned}
 & \int_0^c \alpha(\xi) \{ K_{13}(t, \xi) - K_{14}(t, -\xi) \} d\xi + \int_0^c \overline{\alpha(\xi)} \{ K_{14}(t, \xi) - K_{13}(t, -\xi) \} d\xi \\
 & + \int_0^c \beta(\xi) \{ K_{15}(t, \xi) - K_{16}(t, -\xi) \} d\xi + \int_0^c \overline{\beta(\xi)} \{ K_{16}(t, \xi) - K_{15}(t, -\xi) \} d\xi \\
 & + 2 \int_0^l \frac{\psi(\tau) d\tau}{(t-\tau) e^{i\theta}} + \int_0^l \psi(\xi) K_{17}(t, \tau) d\tau + \int_0^l \overline{\psi(\tau)} K_{18}(t, \tau) d\tau + f_3(t) = 0 \\
 & 0 \leq t \leq l
 \end{aligned} \tag{37}$$

$$\int_0^c [\alpha(\xi) - \overline{\alpha(\xi)}] d\xi = \frac{P}{2\pi i(\kappa + 1)} \tag{38}$$

$$\int_0^c [\beta(\xi) - \overline{\beta(\xi)}] d\xi + \int_0^l [\psi(\tau) - \overline{\psi(\tau)}] d\tau = 0. \tag{39}$$

8. Numerical results and stress-intensity factor analysis

Equations (35)–(39) were numerically solved using the method proposed by Gerasoulis [12]. For the numerical work the symmetry of the problem was not employed, and the procedure for

the pre-cracking case was used, except that two sets of dislocation densities, one along z_2 and another along $-\bar{z}_2$, were used. The numerical work could be checked by observing the symmetries and antisymmetries of the solutions as (6) was enforced. The unknown functions α , β and ψ were assumed such that the singularity of ψ at the tips of the anchor is of an order less than $1/2$ [13]. These conditions render the solution unique.

The stress intensity factors, defined by

$$K_I - iK_{II} = \lim_{\tau \rightarrow l^+} \sqrt{2\pi(\tau - l)} (\sigma_{\phi\phi} - i\sigma_{\rho\phi}) \quad (40)$$

can be related directly to $\psi(\tau)$ by taking the asymptotic form of (37). In terms of dimensionless quantities arising from the numerical scheme, the result is

$$(K_I - iK_{II}) \frac{\sqrt{c}}{P} = \sqrt{2} \pi^{3/2} e^{-i\theta} \sqrt{\frac{l}{c}} \psi^*(1) \quad (41)$$

where

$$\psi(\tau) = \frac{\psi^*(s)}{\sqrt{1-s^2}} \frac{P}{c}; \quad s = \frac{2\tau}{l} - 1. \quad (42)$$

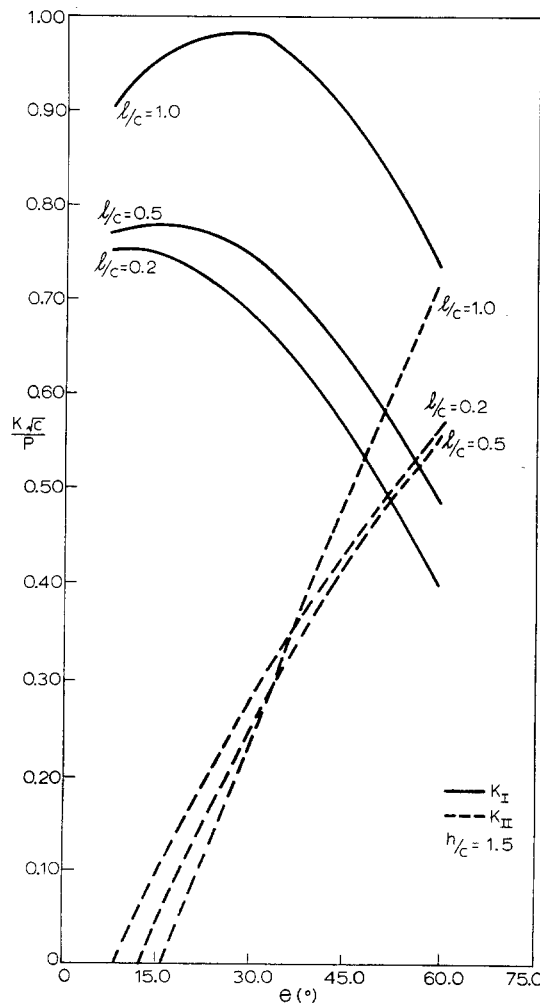


Fig. 6. Stress intensity factors as functions of extension angle ($h = 1.5c$) (from [6]).

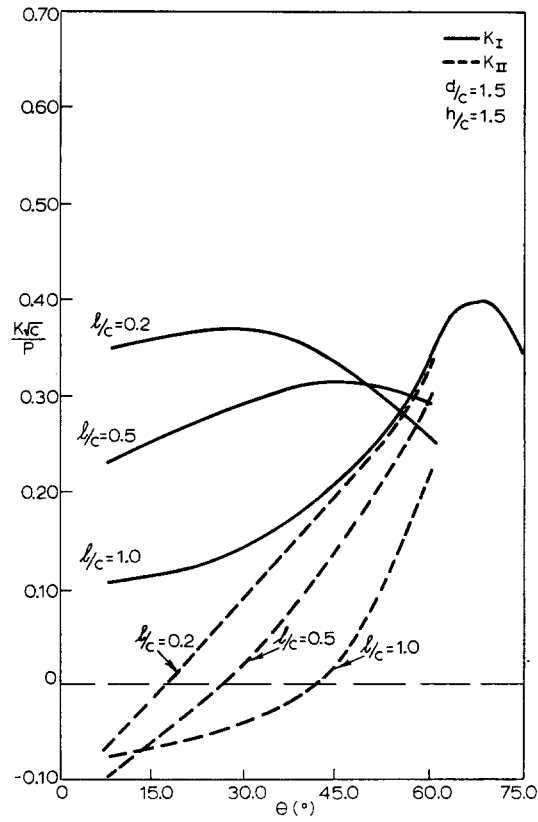


Fig. 7. Stress intensity factors as functions of extension angle ($h = d = 1.5c$) (from [6]).

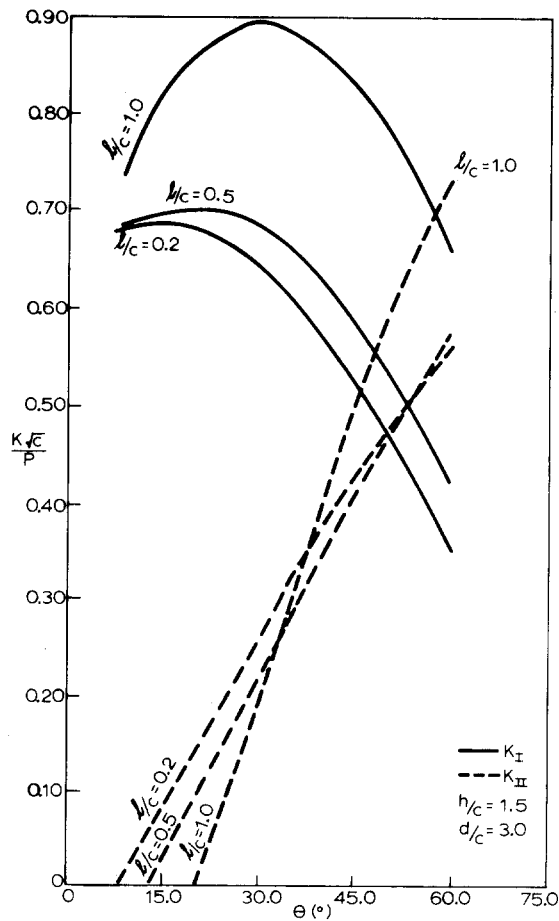


Fig. 8. Stress intensity factors as functions of extension angle ($h = 1.5c$, $d = 3.0c$).

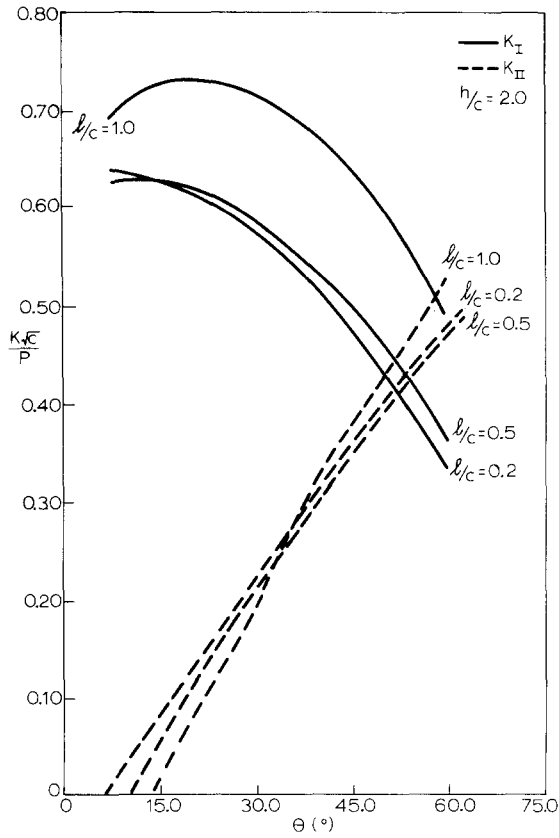


Fig. 9. Stress intensity factors as functions of extension angle ($h = 2.0c$).

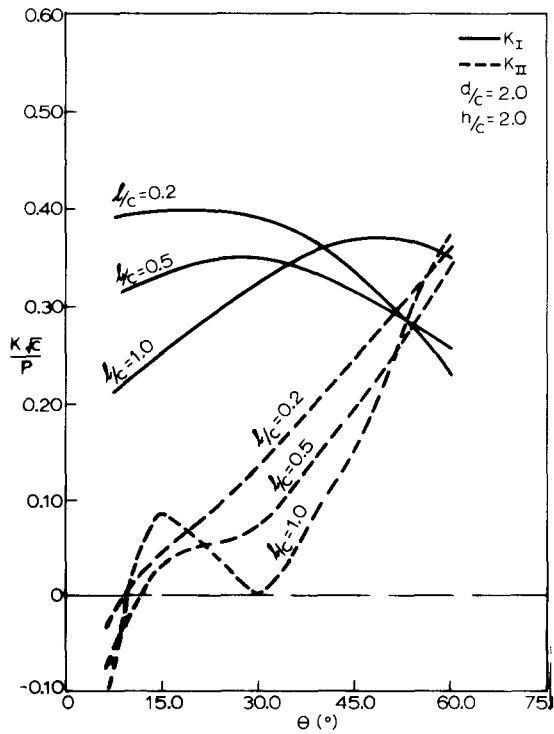


Fig. 10. Stress intensity factors as functions of extension angle ($h = d = 2.0c$).

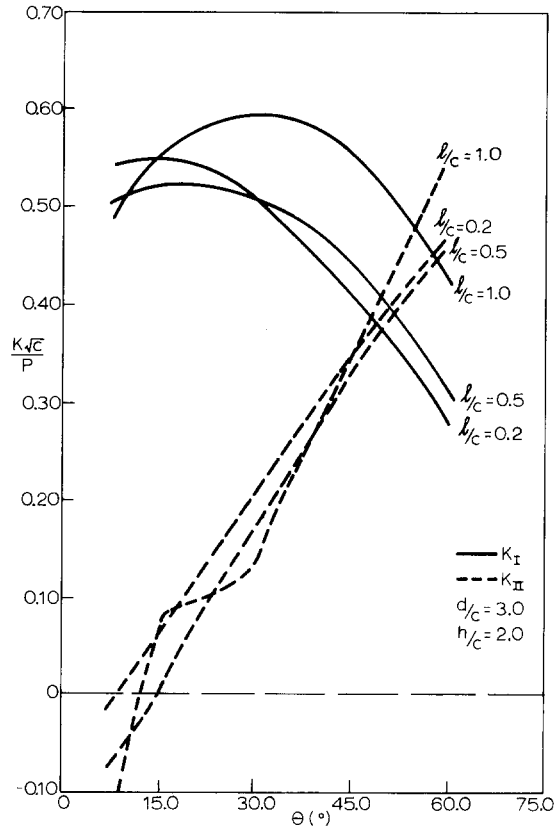


Fig. 11. Stress intensity factors as functions of extension angle ($h = 2.0c$, $d = 3.0c$).

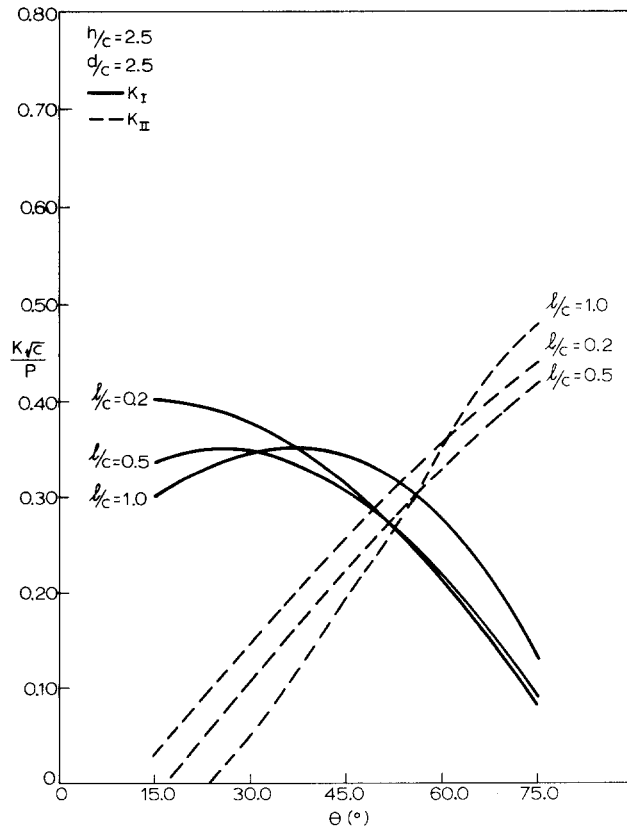


Fig. 12. Stress intensity factors as functions of extension angle ($h = d = 2.5c$).

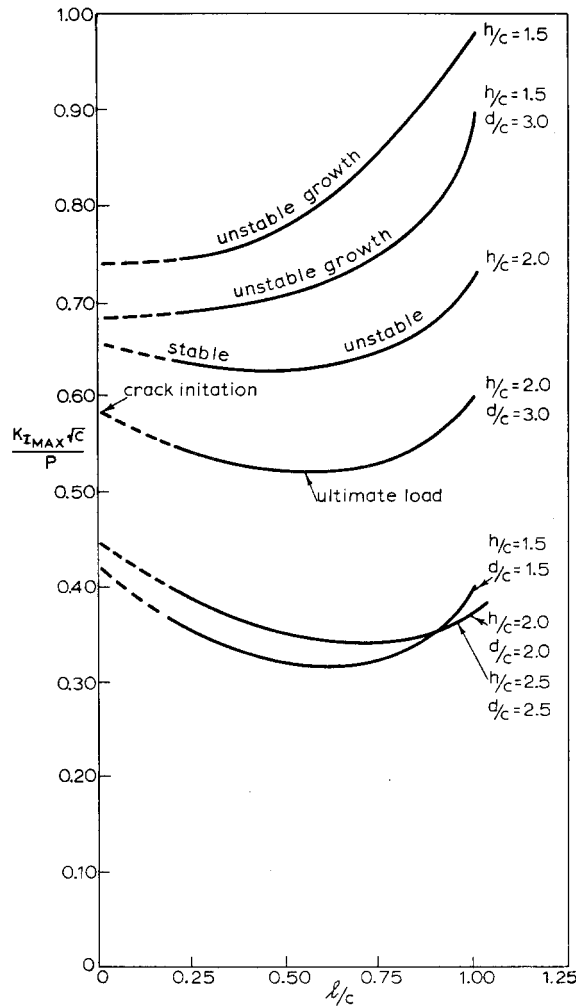


Fig. 13. Maximum mode-I stress intensity factors as functions of crack length (from [6]).

To characterize crack growth during the pull-out process, stress intensity factors were calculated for several combinations of the parameters involving crack length, extension angle, location of the concentrated forces support reactions (top surface) and embedment of the plate. Figures 6–12, which are plots of the stress intensity factors as functions of the crack extension angle for several configurations, present the results of these calculations. The results show that for short cracks the maximum values of the opening mode stress intensity factor (K_I) occur at points where the shear mode factor (K_{II}) is nearly zero. We assume that both crack initiation and the direction that the extended crack will choose to grow are governed by the opening mode (see, for example, Horii and Nemat-Nasser [14]). The anchor pull-out crack initiation direction will therefore be assumed to depend upon the direction of maximum K_I .

Figure 13 is a plot showing the maximum value of the opening mode stress intensity factor versus crack length for several test configurations. The effect of the support reactions on the stability of crack propagation can be clearly seen. For relatively short spacing of the support forces and deep embedments, cracks will grow in a stable manner (an increase in load is needed for additional growth) until they reach l/c values approximately equal to 0.75; after this point they will continue to grow but in an unstable manner. On the other hand, for wide spacing and

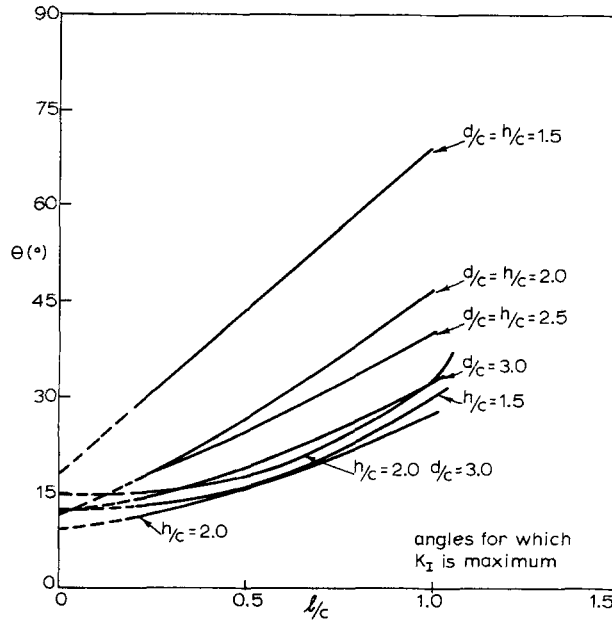


Fig. 14. Angles of maximum K_I as functions of crack length (from [6]).

shallow embedments, crack growth is unstable for all crack lengths. These results are consistent with the experimental results presented in [6].

The approximate method proposed by Horii and Nemat-Nasser was used to predict crack paths. With respect to the xy coordinate system shown in Fig. 1, the crack profile is defined as $x = c + g(r)$, $y = f(r)$, where r is a parameter that measures distance along the crack, and c is the half-length of the plate. Figure 14 is a plot obtained from results such as those in Figs. 6–12 showing the angles of maximum K_I as functions of crack length for several configurations. The angle between the tangent to the curved crack extension and the x -axis is assumed to be $\theta = \theta(l/c)$, so that

$$\frac{df}{dl} = \sin \theta, \quad \frac{dg}{dl} = \cos \theta. \tag{43}$$

The crack profiles shown in Figs. 15–18 were obtained after numerically integrating (43) into which $\theta(l/c)$ from Fig. 14 was substituted.

It can be seen that cracks initiate and grow almost horizontally for short lengths; for $l/2c = 0.1$, θ varies from 10° to 25° , depending on the embedment depth and the spacing of

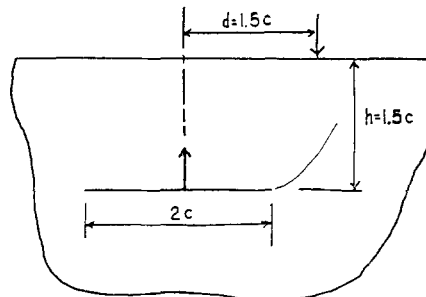


Fig. 15. Predicted crack path ($h = d = 1.5c$).

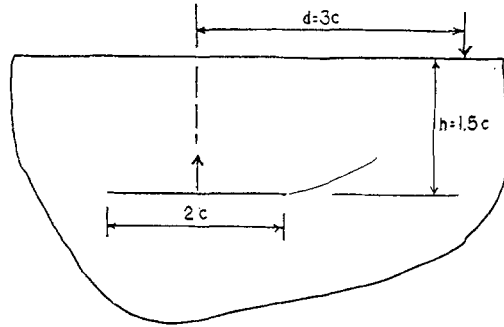


Fig. 16. Predicted crack path ($h = 1.5c$, $d = 3.0c$).

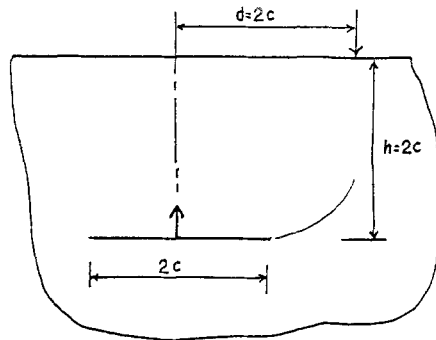


Fig. 17. Predicted crack path ($h = d = 2.0c$).

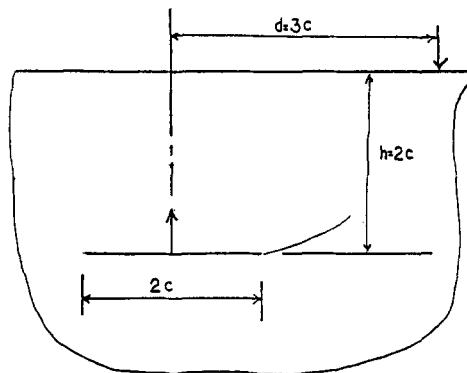


Fig. 18. Predicted crack path ($h = 2.0c$, $d = 3.0c$).

the concentrated forces. As the cracks become longer, they tend to turn and grow towards the supports.

The results presented in this paper are consistent with those obtained from experiments conducted using mortar as a matrix material. The experimental procedure, as well as a detailed comparison of the analytical and experimental results, can be found in [6] and will not be reported here.

References

1. G.R. Miller and L.M. Keer, *Journal of Applied Mechanics* 49 (1982) 768–772.
2. A.P.S. Selvadurai, *Geotechnique* 26 (1976) 603–612.
3. V.K. Luk and L.M. Keer, *International Journal for Numerical and Analytical Methods in Geomechanics* 4 (1980) 215–232.
4. I.N. Zhukovskii, *Prikladnaya Mekhanika* 11, No. 11 (1975) 124–128.
5. S.V. Bosakov, *Prikladnaya Mekhanika* 16, No. 3 (1980) 81–87.
6. R. Ballarini, S.P. Shah and L.M. Keer, *Proceedings Royal Society London A* 404 (1986) 35–54.
7. N.I. Muskhelishvili, *Some Basic Problems in the Theory of Elasticity*, Noordhoff, Leyden, The Netherlands (1954).
8. J. Dundurs, in *Mathematical Theory of Dislocations*, ASME (1969) 70–115.
9. A.E. Green and W. Zerna, *Theoretical Elasticity*, Clarendon Press, Oxford, Great Britain (1960).
10. D.I. Sherman, *Comptes Rendus de L'Academie des Sciences de L'U.R.S.S.* 27, No. 4 (1940) 330–334.
11. G.R. Miller and L.M. Keer, *Quarterly of Applied Mathematics* 42, No. 4 (1985) 455–465.
12. A. Gerasoulis, *Computers and Mathematics with Applications* 8 (1982) 15–22.
13. A.H. England, *International Journal of Engineering Science* 9 (1971) 571–585.
14. H. Horii and S. Nemat-Nasser, *Journal of Geophysical Research* (in press).

Appendix A

$$K_1(x, \xi) = \frac{\kappa}{x - \xi - 2ih} - \frac{1}{x - \xi + 2ih} + \frac{8h^2}{(x - \xi + 2ih)^3}$$

$$K_2(x, \xi) = \frac{2ih}{(x - \xi - 2ih)^2} + \frac{2ih\kappa}{(x - \xi + 2ih)^2}$$

$$K_3(x, \rho) = -\frac{1}{x - \rho - 2ih} - \frac{1}{x - \rho + 2ih} + \frac{8h^2}{(x - \rho + 2ih)^3}$$

$$K_4(x, \rho) = \frac{2ih}{(x - \rho - 2ih)^3} - \frac{2ih}{(x - \rho + 2ih)^2}$$

$$K_5(x, \xi) = \frac{\kappa^2}{x - \xi - 2ih} + \frac{1}{x - \xi + 2ih} - \frac{8h^2}{(x - \xi + 2ih)^3}$$

$$K_6(x, \xi) = \frac{2ih\kappa}{(x - \xi - 2ih)^2} - \frac{2ih\kappa}{(x - \xi + 2ih)^2}$$

$$K_7(x, \rho) = \frac{-\kappa}{x - \rho - 2ih} + \frac{1}{x - \rho + 2ih} - \frac{8h^2}{(x - \rho + 2ih)^3}$$

$$K_8(x, \rho) = \frac{2ih\kappa}{(x - \rho - 2ih)^2} + \frac{2ih}{(x - \rho + 2ih)^2}$$

$$K_9(x, \tau) = \frac{1}{x - c - \tau e^{i\theta}} - \frac{1}{x - c - 2ih - \tau e^{-i\theta}} + \frac{1}{x - c - \tau e^{-i\theta}} - \frac{1}{x - c + 2ih - \tau e^{i\theta}}$$

$$+ \frac{8h(h - \tau \sin \theta)}{(x - c + 2ih - \tau e^{i\theta})^3} - \frac{2i(h - \tau \sin \theta)}{(x + c - 2ih + \tau e^{i\theta})^2} - \frac{2i\tau \sin \theta}{(x + c + \tau e^{i\theta})^2} + \frac{2ih}{(x + c + 2ih + \tau e^{-i\theta})^2}$$

$$K_{10}(x, \tau) = \frac{2i(h - \tau \sin \theta)}{(x - c - 2ih - \tau e^{-i\theta})^2} + \frac{2i\tau \sin \theta}{(x - c - \tau e^{-i\theta})^2} - \frac{2ih}{(x - c + 2ih - \tau e^{i\theta})^2} - \frac{1}{x + c + \tau e^{-i\theta}}$$

$$+ \frac{1}{x + c - 2ih + \tau e^{i\theta}} - \frac{1}{x + c + \tau e^{i\theta}} + \frac{1}{x + c + 2ih + \tau e^{-i\theta}} - \frac{8h(h - \tau \sin \theta)}{(x + c + 2ih - \tau e^{-i\theta})^3}$$

$$\begin{aligned}
 K_{11}(x, \tau) &= \frac{\kappa}{x-c-\tau e^{i\theta}} - \frac{\kappa}{x-c-2ih-\tau e^{-i\theta}} - \frac{1}{x-c-\tau e^{-i\theta}} \\
 &+ \frac{1}{x-c+2ih-\tau e^{i\theta}} - \frac{8h(h-\tau \sin \theta)}{(x-c+2ih-\tau e^{i\theta})^3} - \frac{2i\kappa(h-\tau \sin \theta)}{(x+c-2ih+\tau e^{i\theta})^2} \\
 &+ \frac{2i\tau \sin \theta}{(x+c+\tau e^{i\theta})^2} - \frac{2ih}{(x+c+2ih+\tau e^{-i\theta})^2} \\
 K_{12}(x, \tau) &= \frac{2i\kappa(h-\tau \sin \theta)}{(x-c-2ih-\tau e^{-i\theta})^2} - \frac{2i\tau \sin \theta}{(x-c-\tau e^{-i\theta})^2} + \frac{2ih}{(x-c+2ih-\tau e^{i\theta})^2} \\
 &- \frac{\kappa}{x+c+\tau e^{-i\theta}} + \frac{\kappa}{x+c-2ih+\tau e^{i\theta}} + \frac{1}{x+c+\tau e^{i\theta}} \\
 &- \frac{1}{x+c+2ih+\tau e^{-i\theta}} + \frac{8h(h-\tau \sin \theta)}{(x+c+2ih+\tau e^{-i\theta})^3} \\
 K_{13}(t, \xi) &= \frac{1}{c-\xi+t e^{i\theta}} + \frac{\kappa}{c-\xi+t e^{i\theta}-2ih} - \frac{2ih(1-e^{-2i\theta})}{(c-\xi+2ih+t e^{-i\theta})^2} \\
 &- \frac{e^{-2i\theta}}{c-\xi+2ih+t e^{-i\theta}} - \frac{\kappa}{c-\xi+t e^{-i\theta}} - \frac{8h e^{-2i\theta}(t \sin \theta - h)}{(c-\xi+2ih+t e^{-i\theta})^3} \\
 K_{14}(t, \xi) &= \frac{2ih}{(c-\xi+t e^{i\theta}-2ih)^2} + \frac{(1-e^{-2i\theta})}{c-\xi+t e^{-i\theta}} + \frac{\kappa(1-e^{-2i\theta})}{c-\xi+2ih+t e^{-i\theta}} \\
 &- \frac{2ih e^{-2i\theta}}{(c-\xi+t e^{-i\theta})^2} - \frac{2i e^{-2i\theta}(t \sin \theta - h)}{(c-\xi+t e^{-i\theta})^2} - \frac{2i\kappa e^{-2i\theta}(t \sin \theta - h)}{(c-\xi+2ih+t e^{-i\theta})^2} \\
 K_{15}(t, \xi) &= \frac{1}{c-\xi+t e^{i\theta}} - \frac{1}{c-\xi-2ih+t e^{i\theta}} - \frac{2ih(1-e^{-2i\theta})}{(c-\xi+2ih+t e^{-i\theta})^2} \\
 &- \frac{e^{-2i\theta}}{c-\xi+2ih+t e^{i\theta}} + \frac{e^{-2i\theta}}{c-\xi+t e^{-i\theta}} - \frac{8h e^{-2i\theta}(t \sin \theta - h)}{(c-\xi+2ih+t e^{-i\theta})^3} \\
 K_{16}(t, \xi) &= \frac{2ih}{(c-\xi-2ih+t e^{i\theta})^2} + \frac{(1-e^{-2i\theta})}{c-\xi+t e^{-i\theta}} - \frac{(1-e^{-2i\theta})}{c-\xi+2ih+t e^{-i\theta}} \\
 &- \frac{2ih e^{-2i\theta}}{(c-\xi+t e^{-i\theta})^2} - \frac{2i e^{-2i\theta}(t \sin \theta - h)}{(c-\xi+t e^{-i\theta})^2} + \frac{2i e^{-2i\theta}(t \sin \theta - h)}{(c-\xi+2ih+t e^{-i\theta})^2} \\
 K_{17}(t, \tau) &= \frac{1}{2ih-t e^{i\theta}+\tau e^{-i\theta}} - \frac{2i(h-\tau \sin \theta)}{[2c-2ih+e^{i\theta}(t+\tau)]^2} - \frac{(1-e^{-2i\theta})2i(h-\tau \sin \theta)}{(2ih+t e^{-i\theta}-\tau e^{i\theta})^2} \\
 &- \frac{(1-e^{-2i\theta})}{2c+t e^{-i\theta}+\tau e^{i\theta}} + \frac{(1-e^{-2i\theta})}{2c+2ih+e^{-i\theta}(t+\tau)} - \frac{e^{-2i\theta}}{2ih+t e^{-i\theta}-\tau e^{i\theta}} + \frac{2i(h-\tau \sin \theta) e^{-2i\theta}}{(2c+t e^{-i\theta}+\tau e^{i\theta})^2} \\
 &- \frac{8 e^{-2i\theta}(h-\tau \sin \theta)(t \sin \theta - h)}{(2ih+t e^{-i\theta}-\tau e^{i\theta})^3} + \frac{2i(t \sin \theta - h) e^{-2i\theta}}{(2c+t e^{-i\theta}+\tau e^{i\theta})^2} - \frac{2i e^{-2i\theta}(t \sin \theta - h)}{[2c+2ih+e^{-i\theta}(t+\tau)]^2} \\
 K_{18}(t, \tau) &= \frac{2i(h-\tau \sin \theta)}{(-2ih+t e^{i\theta}-\tau e^{-i\theta})^2} - \frac{1}{2c+t e^{i\theta}+\tau e^{-i\theta}} + \frac{1}{2c-2ih+e^{i\theta}(t+\tau)} - \frac{(1-e^{-2i\theta})}{2ih+t e^{-i\theta}-\tau e^{i\theta}} \\
 &+ \frac{2i(h-\tau \sin \theta)(1-e^{-2i\theta})}{[2c+2ih+e^{-i\theta}(t+\tau)]^2} + \frac{e^{-2i\theta}}{2c+2ih+e^{-i\theta}(t+\tau)} - \frac{e^{-2i\theta}}{2c+t e^{-i\theta}+\tau e^{i\theta}} \\
 &+ \frac{2i(t \sin \theta - h) e^{-2i\theta}}{(2ih+t e^{-i\theta}-\tau e^{i\theta})^2} + \frac{8 e^{-2i\theta}(h-\tau \sin \theta)(t \sin \theta - h)}{(2c+2ih+e^{-i\theta}(t+\tau))^3}
 \end{aligned}$$

$$f_1(x) = \frac{iP}{4\pi} \left\{ \frac{1}{x-ih-d} + \frac{1}{x-ih+d} - \frac{1}{x+ih-d} - \frac{1}{x+ih+d} - \frac{2ih}{(x+ih-d)^2} - \frac{2ih}{(x+ih+d)^2} \right\}$$

$$f_2(x) = \frac{iP}{4\pi} \left\{ \frac{\kappa}{x-ih-d} + \frac{\kappa}{x-ih+d} + \frac{1}{x+ih-d} + \frac{1}{x+ih+d} + \frac{2ih}{(x+ih-d)^2} + \frac{2ih}{(x+ih+d)^2} \right\}$$

$$f_3(t) = \frac{iP}{4\pi} \left\{ \frac{1}{c-ih+te^{i\theta}-d} + \frac{1}{c-ih+te^{i\theta}+d} - \frac{1}{c+ih+te^{-i\theta}-d} - \frac{1}{c+ih+te^{-i\theta}+d} \right. \\ \left. + 2i(t \sin \theta - h) e^{-2i\theta} \left[\frac{1}{(c+ih+te^{-i\theta}-d)^2} + \frac{1}{(c+ih+te^{-i\theta}+d)^2} \right] \right\}$$

Résumé

On présente un modèle de mécanique de rupture linéaire et élastique pour une rupture par arrachement causée par un ancrage rigide noyé dans un matériau fragile. L'ancrage est représenté par une plaque rigide chargée verticalement et partiellement solidaire d'un demi espace élastique. On suppose que la rupture prend naissance d'une fissuration émanant du bord de la plaque.

On réduit le problème d'élasticité bidimensionnelle à la résolution numérique d'un système d'intégrales singulières couplées.

On présente les facteurs d'intensité de contraintes pour diverses combinaisons de géométries de mise en charge, de longueurs de fissure, d'angle de fissuration et de profondeur de fixation. On utilise les facteurs d'intensité de contrainte pour tracer les parcours possibles pour la fissure, et pour déterminer sa stabilité de propagation.